Quasicrystals and their Approximants in 2D Ternary Oxides

Stefan Förster,* Sebastian Schenk, Eva Maria Zollner, Oliver Krahn, Cheng-Tien Chiang, Florian O. Schumann, Alireza Bayat, Karl-Michael Schindler, Martin Trautmann, René Hammer, Klaus Meinel, Waheed A. Adeagbo, Wolfram Hergert, Jan Ingo Flege, Jens Falta, Martin Ellguth, Christian Tusche, Marc DeBoissieu, Matthias Muntwiler, Thomas Greber, and Wolf Widdra

2D oxide quasicrystals (OQCs) are recently discovered aperiodic, but well-ordered oxide interfaces. In this topical review, an introduction to these new thin-film systems is given. The concept of quasicrystals and their approximants is explained for $BaTiO_3-$ and $SrTiO_3-$derived OQCs and related periodic structures in these 2D oxides. In situ microscopy unravels the high-temperature formation process of OQCs on Pt(111). The dodecagonal structure is discussed regarding tiling statistics and tiling decoration based on the results of atomically resolved scanning tunneling microscopy and various diffraction techniques. In addition, angle-resolved ultraviolet photoemission spectroscopy and X-ray photoelectron spectroscopy results prove a metallic character of the 2D oxide.

1. Introduction

2D oxide quasicrystals (OQCs) emanate from research dedicated to functional oxide interfaces. Oxide thin films are known to exhibit a wide range of functionalities. When the film thickness is reduced, the impact of the interfacial layer on the film properties increases and additional functionalities can arise, which extend the materials properties with respect to the bulk counterparts. Famous examples are the voltage-driven magnetization switching in multiferroics[1–3] and the formation of a 2D electron gas at the $LaAlO_3/SrTiO_3$ interface.[4,5]

In addition to these functionalities, the observation of a 2D OQC added long-range aperiodic order to perovskite-derived oxide interfaces—two years after the Nobel prize in chemistry was awarded to Dan Shechtman for the discovery of quasicrystals in metal alloy systems.[6] OQCs form spontaneously from perovskite oxide thin films on a metal substrate with sixfold symmetry.[6,7] These interfaces between a periodic substrate and the aperiodic thin film add a new facet to the known forms of interface epitaxy.

Dr. S. Förster, S. Schenk, E. Maria Zollner, O. Krahn, Dr. C.-T. Chiang, Dr. F. O. Schumann, Dr. A. Bayat, Dr. K.-M. Schindler, Dr. M. Trautmann, Dr. R. Hammer, Dr. K. Meinel, Dr. W. A. Adeagbo, Prof. W. Hergert, Prof. W. Widdra
Institute of Physics
Martin-Luther-Universität Halle-Wittenberg
D-06099 Halle, Germany
E-mail: stefan.foerster@physik.uni-halle.de

Dr. C.-T. Chiang, Dr. M. Ellguth, Dr. C. Tusche, Prof. W. Widdra
Max-Planck-Institut für Mikrostrukturphysik
D-06120 Halle, Germany

Prof. J. Ingo Flege
Applied Physics and Semiconductor Spectroscopy
Brandenburg University of Technology
Cottbus-Senftenberg 03046 Cottbus, Germany

Prof. J. Falta
Institute of Solid State Physics
University of Bremen
Bremen, Germany

Prof. J. Falta
MAPEX Center for Materials and Processes
University of Bremen
Bremen, Germany

Dr. C. Tusche
Peter Grünberg Institut (PGI-6)
Forschungszentrum Jülich
D-52425 Jülich, Germany

Dr. M. DeBoissieu
Univ. Grenoble Alpes, CNRS, SIMaP
F-38000 Grenoble, France

Dr. M. Muntwiler
Paul Scherrer Institut
Villigen, Switzerland

Prof. T. Greber
Physik-Institut, Universität Zürich
8057 Zürich, Switzerland

Quasicrystals are materials without the translational symmetry known to periodic crystals, but with a long-range order and a well-defined rotational symmetry visible in diffraction. Often they exhibit an 8-, 10-, or 12-fold rotational symmetry, which is incompatible with translational symmetry.[8–11] Therefore, fundamental concepts in solid-state physics, e.g., the description of electrons by delocalized Bloch states or the concept of extended phonons do not apply for quasicrystals. This makes this class of materials highly interesting also from a fundamental science point-of-view.

Figure 1a shows the first electron diffraction data of an aperiodic oxide structure. The low-energy electron diffraction (LEED) pattern of the OQC clearly shows a 12-fold symmetric pattern. On the atomic scale, this unique structure is built from motifs of equilateral triangles, squares and rhombs, that arrange in characteristic dodecagons, as seen in the scanning tunneling microscopy (STM) image of Figure 1b.[6] We enroll the formation process of the quasicrystalline layers, which follows a self-limiting encapsulation process of the metal surface by the oxide monolayer known as the strong metal support interaction (SMSI) effect of binary oxides on metals.[12–18] Atomically resolved STM images allow for a detailed understanding of the real space tiling of OQCs. It will be demonstrated how a statistical analysis of the real space tiling can be used to identify the Niizeki–Gähler tiling (NGT) as the idealized model system which describes the structure.[19–21] Recursion rules for the NGT are discussed and it is described how the self-similarity, which follows directly from recursion, is altered in the as grown OQC due to phason flips.[21,22] In addition to the real space structure, insights into various diffraction experiments are given. With respect to the electronic structure, we present evidence for unpaired electron spins at the vertices of the dodecagonal tiling as derived from angle-resolved photoemission.[23] Today OQCs can be prepared as perfect monolayer extending over the entire substrate surface and have been successfully tested as template for adsorption experiments.[24,25]

In the field of quasicrystals, a variety of approximant structures are frequently found. These are long-range periodic structures in which the tiling elements or even larger patches of the quasicrystal tiling are cut and form the repeating unit cell. For the ternary oxide monolayers, a variety of approximants to the
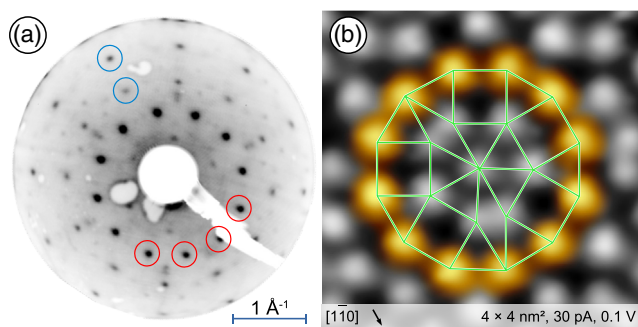
Stefan Förster received his Ph.D. in physics in 2012 at the Martin-Luther-Universität Halle- Wittenberg (MLU). He was awarded a P.R.I.M.E. postdoctoral fellowship of the German Academic Exchange Service and worked from 2014 to 2016 in the group of Greber and Osterwalder at the University of Zurich. Since 2016, he is leading a young researchers group focusing on oxide quasicrystals in the group of Wolf Widdra at the MLU.

Eva Maria Zollner graduated in physics at the Martin-Luther-Universität Halle-Wittenberg. Her Ph.D. in the surface science group at the MLU is devoted to the growth of 2D oxide quasicrystals and their use as templates for molecular adsorption studies.

Wolf Widdra received his Ph.D. in physics in 1991 at the Philipps-Universität Marburg. After a Post-doc at the UC Santa Barbara, he became an Assistant Professor in the group of Dietrich Menzel at the TU Munich in 1994. From 2001 to 2003, he worked as an Associate Professor at the TU Berlin and headed the Department "Synchrotron Radiation, Micro- and Nanostructures" at the Max Born Institute for Nonlinear Optics and Short Pulse Spectroscopy in Berlin. Since 2003, he is a Full Professor at the Martin-Luther-Universität Halle-Wittenberg as head of the Surface Science department.

dodecagonal NGT have been reported.[7,26–31] With increasing size of the unit cell of the approximant, the structures resemble the OQC more closely. Approximants are of special interest due to their periodic nature, as the Bloch theorem applies here and all standard methods of solid-state physics can be used. Especially, surface X-ray diffraction (SXRD) investigations have proven to be most valuable for establishing a complete structural model for OQCs, that goes beyond investigations of the Ti sublattice seen in STM images.[28–30]

2. Preparation and Stability

For the preparation of OQCs, less than 1 nm of a given ternary oxide needs to be deposited on the Pt(111). By annealing the oxide layer at temperatures above 900 K, the material rearranges at the surface, which ultimately can lead to the OQC formation. This structural transformation process has been studied in great detail for the prototypical OQC system of $BaTiO_3$ on Pt(111).[12,32,33] For temperatures around 900 K, a long-range

Figure 1. a) Dodecagonal low-energy electron diffraction pattern of the 2013 discovered oxide quasicrystal derived from $BaTiO_3$ on Pt(111) and b) scanning tunneling microscopy image with the characteristic building blocks marked for the dodecagonal OQC ($4 \times 4\,nm^2$). Adapted with permission.[6] Copyright 2013, Springer Nature.

ordered BaTiO$_3$(111) structure develops. Upon annealing to higher temperatures under oxidative conditions, BaTiO$_3$ tends to reduce the interfacial contact to Pt, which results in the growth of 3D islands. In surplus of oxygen, all BaTiO$_3$ segregates in the islands with bare Pt(111) between the islands. Recently, it has been found that depending on the islands' thickness, a hexagonal BaTiO$_3$ structure can be stabilized in the islands, rather than a simple perovskite stacking along the (111) directions.[34] This structure is the high-temperature phase of bulk BaTiO$_3$.[35]

Under reducing conditions, the annealing of a periodic or amorphous BaTiO$_3$ layer leads to islands formation as well. However, in this case, the Pt(111) substrate will be covered by an ultrathin BaTiO$_{3-x}$ wetting layer. **Figure 2** shows a series of in situ low-energy electron microscopy (LEEM) images of this wetting process for an area of $1.4 \times 1.4\,\mu m^2$. The bright area in the top left image corresponds to bare Pt(111); the gray contrast resembles BaTiO$_3$(111) islands. The faint wavy horizontal lines are the substrate step edges. The wetting layer starts to form locally at the rim of the BaTiO$_3$(111) islands at 1020 K and appears with darker contrast in the LEEM images of Figure 2. Due to the enhanced mobility at the substrate step edges, a growth front of the wetting layer starts there, which connects the local patches to a homogeneous layer with time. At 1020 K, this wetting layer is amorphous. It fully covers the Pt(111) substrate as confirmed by the suppression of the surface core-level shift of Pt in photoemission experiments using synchrotron radiation.[12] Upon temperature increase, a series of

long-range ordered structures is formed in the wetting layer. The OQC is typically found for temperatures ranging from 1070 to 1170 K.[6,12,24,28] At higher temperatures, the film rearranges into a small unit cell periodic approximant structure, which will be discussed in detail in Section 6.

This wetting process can be reversed by reoxidation as shown in the lower sequence of LEEM images in Figure 2. The OQC layer itself is stable against dosing 10^{-6} mbar of molecular oxygen at 900 K. However, with time the bright contrast of the Pt(111) substrate becomes visible and the wetting layer transforms into tiny BaTiO$_3$ islands (bottom left). Due to the initiation at the step edges and the auto-catalytic character, the dewetting is attributed to a reoxidation of the wetting layer using atomic oxygen, that results from a dissociation at Pt sites.[12] The wetting and dewetting cycle shown in Figure 2 is completed by annealing to higher temperatures in O$_2$. This reduces the island density due to Ostwald ripening and coalescence. This cycling is fully reversible. For the case of BaTiO$_3$ on Pt(111), even upon multiple cycling, no Ba or Ti is lost by re-evaporation from the surface or diffusion into the Pt bulk.

For the preparation of OQC films, no special deposition technique is needed. Surface roughening as a consequence of sputter deposition or pulsed-laser deposition will not hinder the OQC formation, as surface defects will be healed out during the high-temperature treatment involved in the OQC formation process. However, the highest level of precision in the preparation of OQC monolayers has been reached using molecular beam
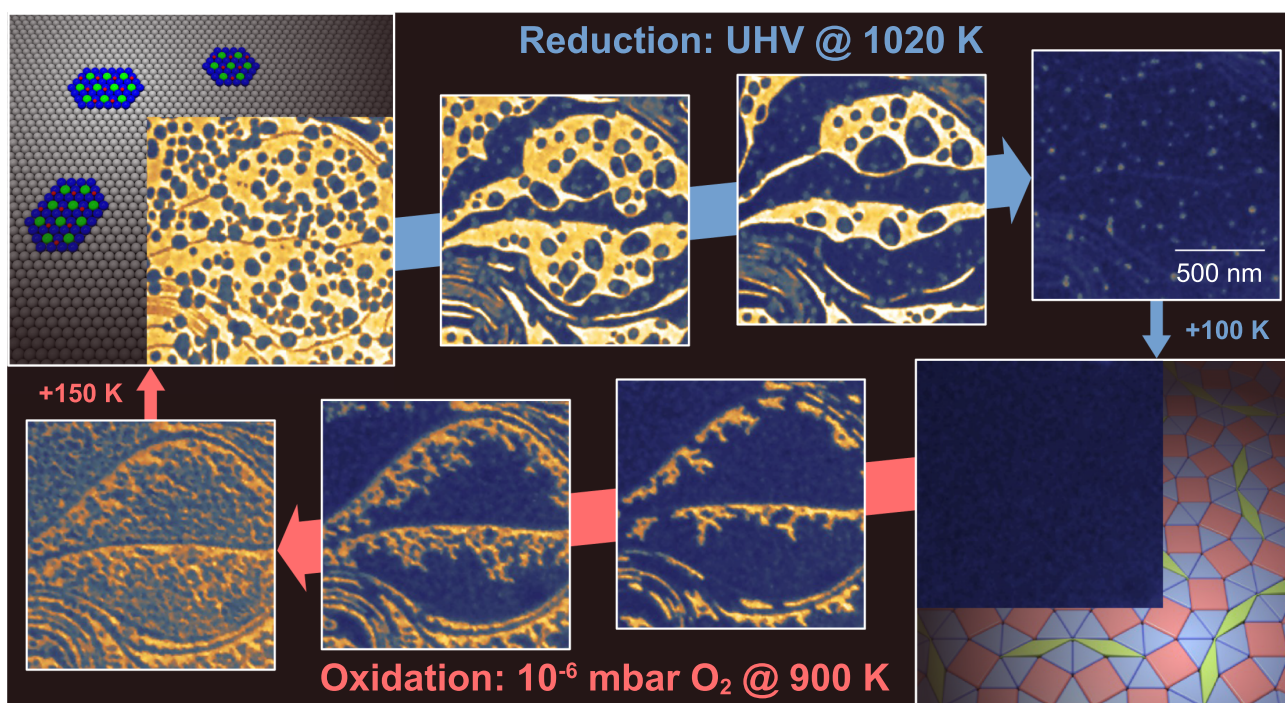

Figure 2. In situ LEEM observation of the wetting and dewetting process of a monolayer of BaTiO$_3$ on Pt(111). At 1020 K, small hexagonal BaTiO$_3$(111) islands on bare Pt (top left) are transformed into a complete wetting layer encapsulating the metal surface (top right) under reducing conditions. This proceeds by a spreading of the material from the 3D islands across the Pt substrate in a 2D layer, which continuously grows with time to full coverage. At 100 K higher UHV annealing temperature, this wetting layer develops into the homogeneous dodecagonal OQC (bottom right). For high oxygen chemical potentials, the OQC decays into smallest BaTiO$_3$ islands (bottom left). This process starts from the substrate step edges and destroys the wetting layer in a dendritic fashion. At 150 K higher temperatures, the small islands grow by coalescence and ripening, which closes the redox-cycle. A movie of this transition is available in the Supporting Information.

epitaxy (MBE).[24] By calibrating independent Ba and Ti sources using a quarz-crystal micro balance (QMB), the right composition and coverage can be guaranteed. As demonstrated in this issue by Zollner et al., perfect monolayers can be grown that extend over the entire surface, which have been already successfully tested as templates for molecular adsorption.[24,25]

When depositing more than the required monolayer BaTiO₃ equivalent or having an off-stoichiometric metal composition, a phase separation occurs at the substrate surface. In coexistence to the OQC, the excess material will form additional islands of perovskite-related structures. For the BaTiO₃/Pt system, it turned out that the OQC will be formed for higher coverages even if the overall metal composition varies by ±15% around the stoichiometric value. This implies that the OQC stoichiometry is fixed and the islands can act as a materials reservoir that compensates deviations from the optimal composition. This formation of 2D wetting layers of reduced ternary oxides in coexistence with 3D islands is not unique for BaTiO₃ on Pt(111). It has also been reported recently for SrTiO₃ on Pt(111) as well as BaTiO₃ on Ru(0001) and emphasizes a rather universal scheme for ternary oxides on metals.[7,31]

3. Electronic Structure

According to the preparation conditions for the wetting and dewetting cycle introduced earlier, the OQC should have a reduced character. This is confirmed by the Ti-2p core-level binding energies. **Figure 3** shows two X-ray photoelectron spectroscopy (XPS) spectra of the Ti-2p region for a 1 nm thin BaTiO₃ film on Pt(111) after 3D island formation and rewetting. The two spectra have been recorded with synchrotron radiation at photon energies of 670 and 1000 eV, respectively.[36] The spectra are normalized to the low binding energy background and offset for clarity. At the given film thickness, a coexistence of BaTiO₃ islands with a periodic structure and the OQC is observed upon ultrahigh vacuum (UHV) annealing, as confirmed by LEED (not shown). In these two structures, the titanium atoms are chemically different as evidenced by XPS, which shows a superposition of two Ti-2p doublets. For the higher binding energy component, the Ti-2$p_{3/2}$ peak is centered at 459.0 eV. For the lower binding energy component, this peak is observed at 456.3 eV. The doublet at 459.0 eV
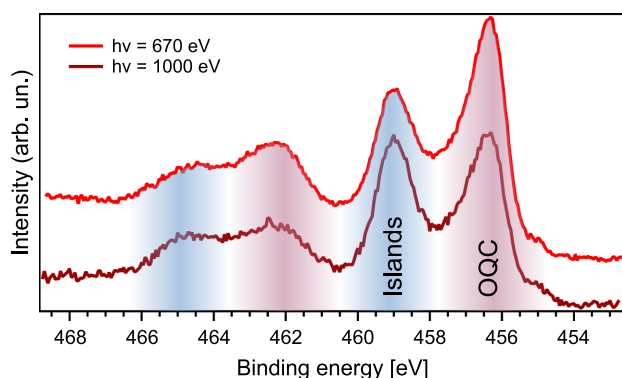
is assigned to the BaTiO₃ islands, as its binding energy is in perfect agreement with that of Ti⁴⁺ in bulk BaTiO₃.[37] The intensity decrease in this component upon reducing the photon energy as observed in Figure 3 furthermore confirms that this signal relates to 3D islands. The large downshift in energy of 2.7 eV for the second component, which corresponds to Ti atoms in the OQC, clearly indicates a reduction of this 2D layer. However, this shift is much larger than typically observed for reduced BaTiO₃ or TiO₂. There the introduction of oxygen vacancies causes the formation of a Ti³⁺ component, which is shifted by maximal 2 eV.[37–39] A shift that is comparably large as for the OQC has been reported for Ti ions in 2D binary oxides on metal surfaces.[40–43] The energetic position might also reflect a distinct variation in the binding geometry rather than a formal oxidation state. As a consequence of the reduction, Ti-3d states that are located at the Fermi level are filled, which induces a metallic character to the OQC layer. A first hint toward this direction comes from a peak asymmetry of the OQC component, which can be well described using a Doniach–Sunjic line shape.[44]

The direct evidence of the metallic character of the OQC comes from angle-resolved photoemission using momentum microscopy.[23] **Figure 4** shows 2D momentum maps of the bare and the OQC covered Pt(111) substrate, recorded at the Fermi energy and at 0.5 eV binding energy. In the presence of OQC, the signature of the Pt bulk bands remains clearly visible, although these features are damped by the 2D overlayer. In addition, the OQC induces a strong enhancement of the photoelectron intensity around the $\bar{\Gamma}$ point at the Fermi level. Its energetic and momentum position nicely matches that of occupied Ti-3d states in oxygen-deficient BaTiO₃ films forming 2D electron gases.[45] With increasing binding energy the intensity distribution becomes narrower indicating an $E(\vec{k})$ dispersion of the Ti-3d states

Figure 3. XPS data for the Ti-2p core level region for the OQC in presence of BaTiO₃(111) islands. Due to the increased surface sensitivity at 670 eV photon energy, the photoelectron intensity of the 3D islands is reduced.
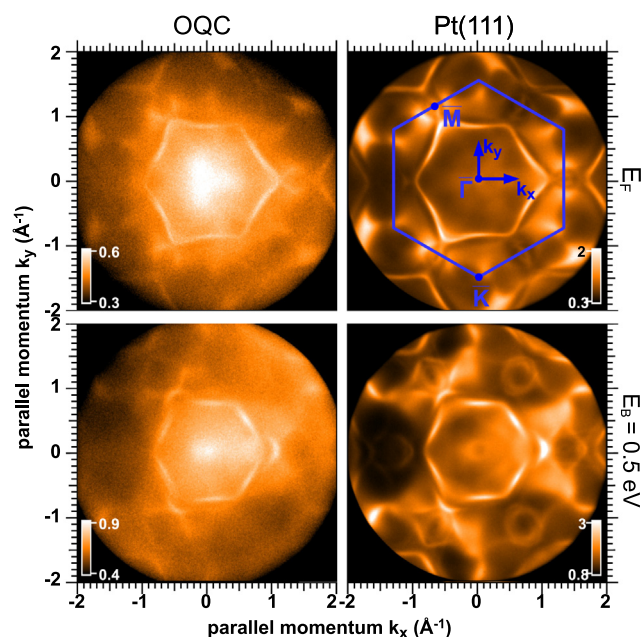
Figure 4. Comparison of the 2D momentum maps of the BaTiO₃-derived OQC on Pt(111) and of the bare Pt(111) substrate at the Fermi energy and 0.5 eV below. Color scale in 10⁴ CCD counts.

of the OQC. Regarding the filling of the Ti-3d states, the Fermi wave vector has been estimated. From the full-width-at-half-maximum of the momentum distribution along the k_y direction, a lower bound of the Fermi wave vector of 0.4 Å^{-1} could be estimated. This value is consistent with the 0.6 Å^{-1} of a $3d^1$ configuration for each Ti atom within the OQC structure and in agreement with the reduction seen by XPS.[23] The assignment of an unpaired electron spin on each Ti site is an exciting finding, which paves the way into future studies of the magnetic ordering in the OQC layer.

4. Real Space Structure

The real space structure of the OQC has been determined from atomically resolved STM images. **Figure 5** shows an example on
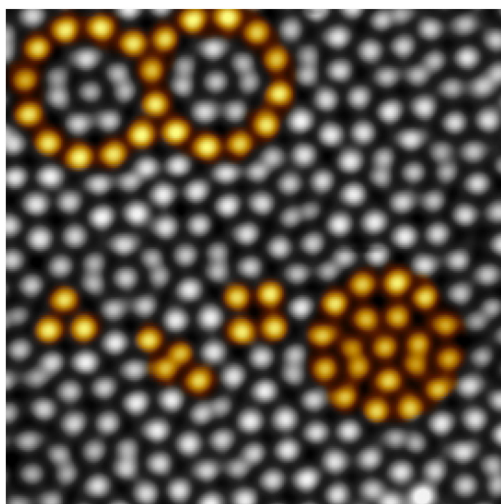

Figure 5. Atomically resolved STM image of the BaTiO₃-derived OQC on Pt(111). The structure forms from three different tiling elements that build a characteristic dodecagon. The 2D tiling is created from overlapping dodecagons. The coloring has been added to emphasize the building blocks. 10 × 10 nm², 30 pA, −0.15 V.

the scale of 10 × 10 nm². The OQC appears as bright protrusions with an interatomic spacing of 6.85 Å. This imaging contrast is robust upon bias voltage variations away from the Fermi level and does not depend on bias polarity within a range from −1.0 to 1.0 V.[6] These tunneling characteristics can be explained by tunneling out or into the Ti $3d$ states, which is in line with the photoemission results. A detailed inspection of the atomically resolved features in the STM image reveals three different tiling elements within the OQC: equilateral triangles, squares, and rhombs inclining 30° and 150° angles. The vertices of these tiling elements are decorated by Ti. These three tiling elements are frequently found in groups of twelve triangles, five squares, and two rhombs that arrange in a characteristic dodecagon as emphasized in color in Figure 5. The 2D layer builds up from overlapping dodecagons.

A mathematical description of a 2D dodecagonal quasicrystal with these building blocks has been reported by Niizeki, Mitani, and Gähler in the late 1980s, why we denote this structure as the NGT.[19,20] This tiling can be generated by the cut-and-project method from a 4D periodic lattice, which is the general scheme to rationalize quasicrystals.[46–48] Alternatively, it can also be generated by recursion.[22] The recursion rule is shown in **Figure 6**a. In each deflation step, a triangle is substituted by seven triangles and three squares of smaller length. Each square is replaced by 16 triangles, five squares, and four rhombs. The rhombs are replaced by eight triangles, two squares, and three rhombs. The shaded areas in the rhombs and the squares indicate, that a given orientation of these tiles needs to be respected, which reduces their symmetry.[21,22] Mathematically, this substitution rule can be formulated by a deflation matrix T

$$T = \begin{pmatrix} 7 & 16 & 8 \\ 3 & 5 & 2 \\ 0 & 4 & 3 \end{pmatrix}. \tag{1}$$

The rows of T are assigned to the number of triangle, square, and rhomb tiles in each replacement, respectively. The Eigensystem solution of T reveals two important properties of
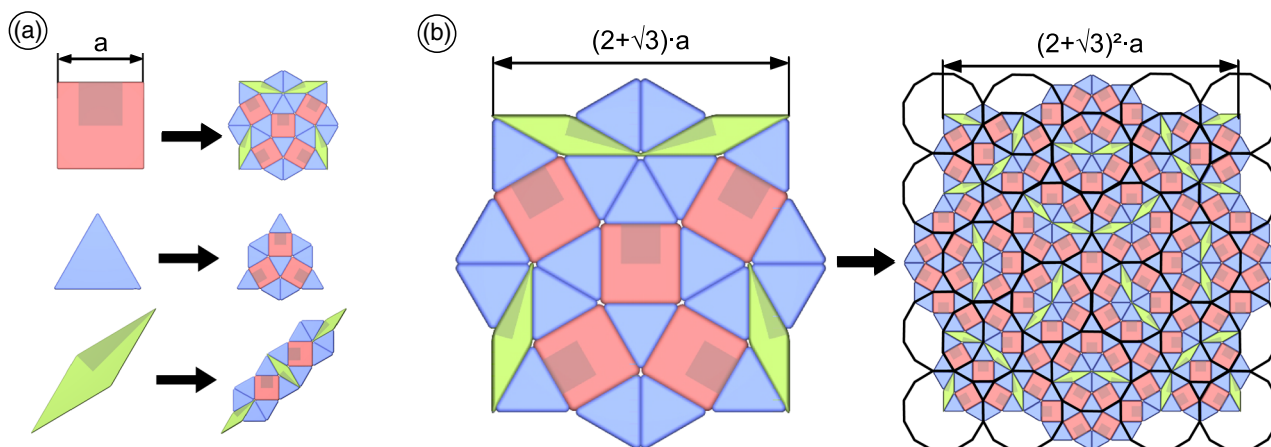

Figure 6. Substitution rules for the dodecagonal NGT: a) First recursion step.[22] b) Second recursion step for the square element: By multiple iterations, the recursion generates self-similar tilings that scale with $(2 + \sqrt{3})$. The higher-hierarchical tiling connects the centers of dodecagons formed in the lower generation instance (black circles).

the NGT: The square root of the eigenvalue gives the scaling factor of self-similarity in the NGT of $(2 + \sqrt{3})$. Furthermore, the corresponding Eigenvector of the deflation matrix T

$$((1 + \sqrt{3}), 1, (1 + \sqrt{3})^{-1}) \approx (2.73, 1, 0.37) \qquad (2)$$

represents the tiling element ratio in the NGT: the numbers of triangles relative to the numbers of squares and of rhombs. This ratio can be used to derive other entities that can be used for a statistical analysis of the NGT, e.g., the frequency of shared edges between the different tiles.

Figure 6b shows that the subsequent application of the recursion rule not only increases the size of the grown patch according to the scaling factor but also results in a self-similarity of the tiling. In the third-generation tiling shown in Figure 6b on the right, the subsequent application of the recursion rule has led to the formation of characteristic dodecagons of the NGT. By connecting the centers of these dodecagons, a triangle-square-rhomb tiling is formed on next-larger scale as emphasized in black in Figure 6b.

Recently, a systematic statistical analysis of the BaTiO$_3$-derived OQC tiling has been conducted for a system of 8100 vertex positions as determined from an atomically resolved large-scale STM image.[21] In this issue, Zollner et al. repeat this analysis for an even larger dataset of almost 20 000 vertices.[24] The comparison of both systems to the statistics of the ideal NGT regarding tiling element ratio and frequency of shared edges clearly reveals that the OQC is the first realization of this ideal dodecagonal model system. To the best of our knowledge, these are the largest real space datasets of any quasicrystal analyzed so far.

First of all, an almost perfect match of the OQC tiling element ratios of 2.75:1:0.36 (8100 vertices) and 2.75:1:0.38 (20 000 vertices) to that of the ideal NGT of 2.73:1:0.37 has been found. Even more intriguing is the superior agreement in the frequency of shared edges. **Figure 7** summarizes the values obtained for the three systems. In the NGT, only triangle-square, triangle-triangle, and triangle-rhomb edges occur. Their relative frequencies agree perfectly with those of the experimentally determined ones for the real OQC. Due to defects that are intrinsically present in real systems, also rhomb-rhomb, rhomb-square, and square-square
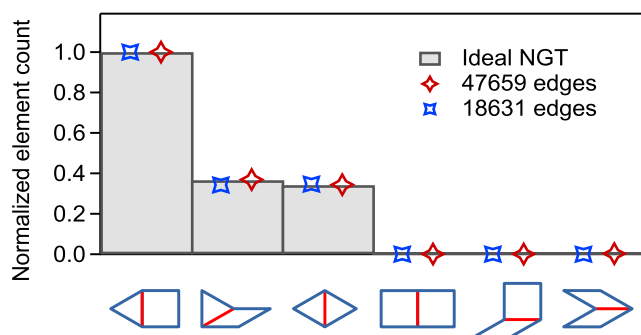
edges occur. However, they amount to 12 out of 18 631 edges (8100 vertices) and 128 out of 47 659 (20 000 vertices) in total, which is a remarkably low number of defects and underlines the perfectness of quasicrystalline order here.[21,24]

Deviations of the OQC statistics from the NGT have been reported with respect to the rotation of rhombs and dodecagons.[21] The combination of both facts, namely, variations in the rotation of building blocks and an ideal edge frequency, points toward a significant amount of phason flips in the tiling. Phasons flips are changes of vertex positions in real space between well-determined positions as a consequence of excitations in the higher-dimensional hyperspace.[49–51] This small displacement of a vertex results in exchanged positions of the surrounding tiles. Please note that the edge-sharing frequencies of the NGT are preserved upon single phason flips. In this way, the quality of the quasicrystal can be assessed in the presence of the specific disorder of phason flips.

The presence of phason flips makes the recognition of the higher-hierarchical tiling in STM images more challenging. By neglecting the location and the orientation of rhombs and locating rings of twelve atoms that create a framework of adjacent dodecagons, the higher-hierarchical tiling were identified in **Figure 8**a. For a better comparison to the ideal NGT, the selected area in the STM image corresponds to the tiling shown on the right in Figure 6b. The Ti atomic positions of the OQC
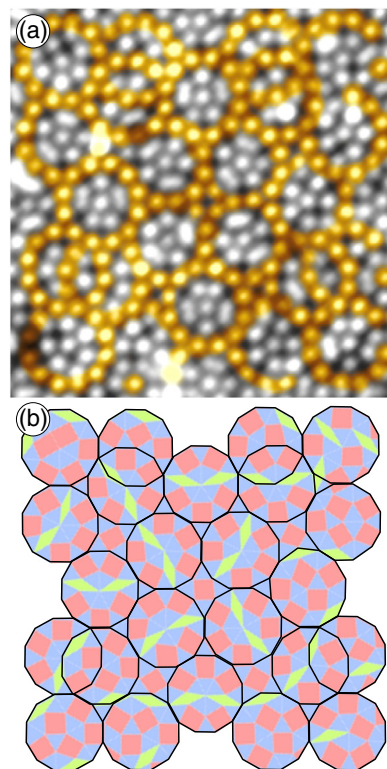
Figure 8. a) The higher-hierarchical tiling of the BaTiO$_3$-derived OQC measured by STM and b) the corresponding tiling scheme. Rings of 12 atoms at the outer ring of the characteristic dodecagons are emphasized in yellow color in the STM image and as black rings in (b). The apparent disorder in the orientation of rhombs within these dodecagons is caused by phason flips. (a) 13×13 nm^2, 25 pA, 1.0 V.

Figure 7. Statistical analysis of the OQC based on STM images: Frequencies of shared edges between adjacent tiles in the mathematically defined NGT (bars) and for two extended data sets of different OQC preparations on different Pt(111) crystals (red and blue marker).[21,24]

tiling as extracted from the STM image are shown in Figure 8b. It clearly indicates strong deviations of the inner structure of the characteristic dodecagons from the ideal NGT. For only half of the dodecagons, the two rhombs point toward the center in agreement with the NGT. For all the others, at least one of the rhombs has moved toward the rim or even left the dodecagon. This motion of rhombs is the signature of multiple phason flips.

5. Diffraction

Oxide quasicrystals were discovered due to the observation of a twelvefold-symmetric diffraction pattern in LEED, as shown for the example of the $BaTiO_3$-derived OQC on Pt(111) in Figure 1 and **9a**. This clear dodecagonal pattern, instead of diffraction rings, reports on an epitaxial alignment of the OQC along the high-symmetry directions of the substrate. The LEED pattern of the OQC is characterized by twelve sharp and intense spots at $1.03\,Å^{-1}$ as shown in Figure 9a, which has been recorded by spot-profile analysis low-energy electron diffraction (SPALEED). The intense spots correspond to the second diffraction order, in correction to the initial report in ref. [6]. Indeed, the first-order spots are only seen at kinetic energies below 10 eV (not shown here). Two additional rings of twelve spots are found at larger **q** vectors under a rotation of 15° with respect to the first ring. Additionally, close to the first-order spots of the Pt substrate pairs of spots occur in twelve directions. In addition to this characteristic dodecagonal pattern, the sixfold symmetry of the substrate leads to a backfolding of intense QC spots from neighboring surface Brillouin zones of the hexagonal substrate, as has been explained in great detail recently.[24] The backfolding at the substrate superimposes a sixfold symmetric pattern to the original dodecagonal diffraction of the OQC. An

example for a backfolded spot, which is extraordinary intense at the given electron kinetic energy, is marked by the black open circle in Figure 9a.

An alternative approach to the momentum space can be obtained from FT of atomically resolved STM images as shown in Figure 9b for a dataset with 20 000 atomic positions. The use of identical scatterers at these atomic coordinates results in a reduced background on the FT and unravels the long-range dodecagonal symmetry of the OQC tiling nicely. In comparison to the LEED pattern of Figure 9a, many higher diffraction orders of nonzero intensity are seen in the FT. Keeping in mind that the FT was calculated from the Ti subgrid only, whereas the LEED pattern additionally contains the information about the Ba and O grids; the lower number of observed spots in LEED points toward systematic extinction of diffraction spots.

The diffraction pattern of the ideal and infinitely extended NGT is shown in Figure 9c. It has been derived by Fourier transforming the acceptance domain of the NGT in internal space.[20,52] Positions and intensities of the diffraction peaks of the NGT in Figure 9c agree reasonably with the FT in Figure 9b. Surprisingly, the relative intensities of the three inner rings of 12 spots seen in LEED are also in good agreement with those of the NGT tiling. From the additional atomic decoration of the NGT by Ba and O, larger intensity differences are expected as compared with the pure Ti grid.

One way to possibly access the tiling decoration is the use of SXRD. There, due to the small scattering cross-section of the X-rays, only single scattering needs to be considered. Consequently, the measured intensities can be directly compared with model calculations. A reciprocal space map of the $BaTiO_3$-derived OQC on Pt(111) measured by SXRD is shown in **Figure 10**. The small full-width-at-half-maximum of the OQC in the order of $0.03\,Å^{-1}$ reports of the high quality of the
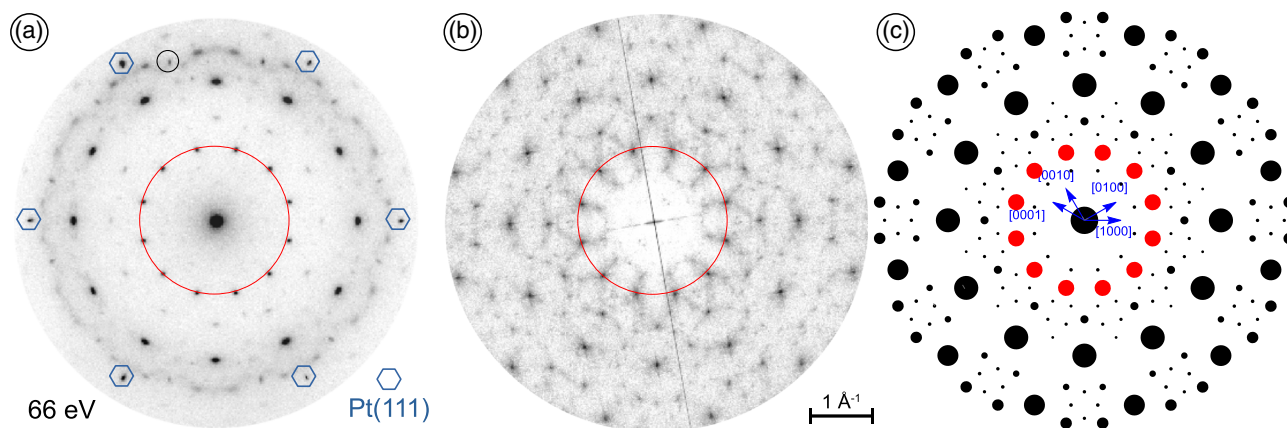

Figure 9. a) Low-energy electron diffraction of the $BaTiO_3$-derived OQC on Pt(111) (SPA-LEED at 66 eV). b) FT of an atomically resolved STM image with almost 20 000 Ti atoms. c) Calculated diffraction pattern of the ideal NGT. The second-order diffraction is marked in red for comparison. The black open circle in (a) emphasizes a backfolded spot originating from the next Brillouin zone of the Pt(111) substrate.
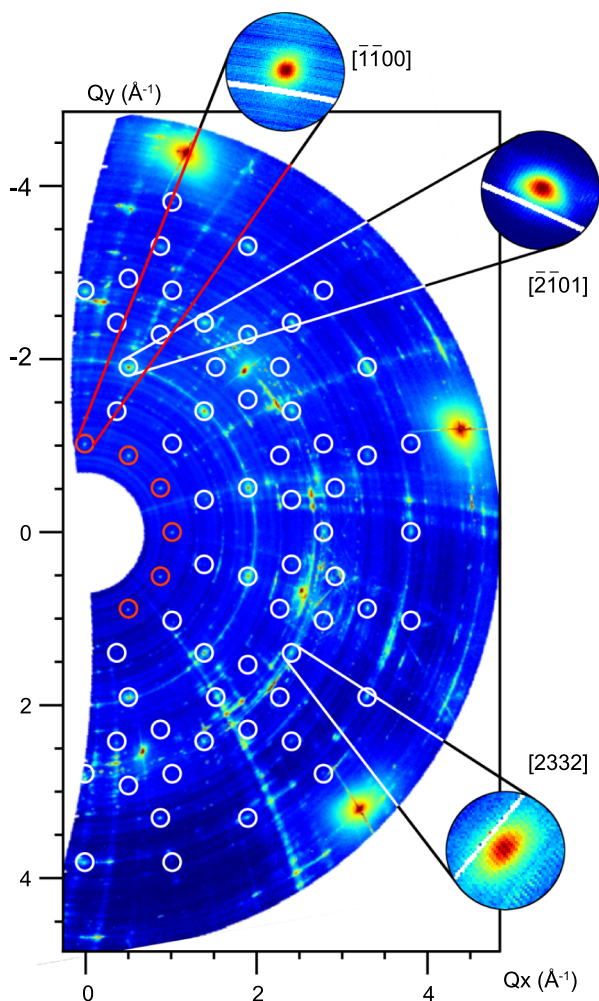
Figure 10. Reciprocal space map of the $BaTiO_3$-derived OQC on Pt(111) measured by SXRD. The circles emphasize the diffraction spots of the OQC. The second-order diffraction spots are marked in red. The three Bragg peaks $[\bar{1}\bar{1}00]$, $[\bar{2}\bar{1}01]$, and $[2332]$ are shown on a $20\times$ enlarged scale in the insets from top to bottom, respectively.

dodecagonal layer. The establishment of a complete structural model of the OQC is one of the current topics of research on this system. Note that the theoretical model reported by Cockayne et al. is able to predict a dodecagonal Ba–Ti–O structure with a $Ba_{0.37}Ti_1O_{1.55}$ stoichiometry where the NGT is formed by the Ba atoms.[27] Experimentally, we find a stoichiometry close to $Ba_1Ti_1O_{3-x}$ and observe a NGT in STM, which is formed by Ti atoms.

6. Approximants

A common scheme to all quasicrystal systems is their formation within a small temperature window in the multidimensional composition phase diagram. Upon deviations from the optimal formation conditions of quasicrystals, periodic structures are typically formed that are created from the same building blocks

as the related quasicrystal. They often have unit cells that are smaller or larger patches of the parent aperiodic structure and are called approximants. Also for OQCs, such approximants have been reported as shown in **Figure 11**.[7,26,28,29,31] Within the ideal NGT shown in Figure 11a, two clusters are highlighted. By translating these clusters along two unit vectors in the plane, periodic tilings arise as shown in Figure 11b,c. The larger the cluster is, i.e., its unit cell, the closer it resembles the aperiodic structure.

The small unit cell approximant shown in Figure 11b was observed for the $BaTiO_3$/Pt system.[28,29] This triangle-square tiling is called σ-phase approximant or snub-square tiling and contains a combination of six tiles as found in the OQC. It is also known as $3^2.4.3.4$ Archimedean tiling[53] and was described for the first time 400 years ago by Johannes Kepler.[54] On the Pt(111) substrate, it forms a commensurate superstructure under 8° rotation out of the substrate high-symmetry directions. By a combination of STM, LEED, SXRD, and calculations by means of density functional theory (DFT), its structure has been determined as also presented in this issue by Meyerheim et al.[28,30] The same superstructure has been observed recently for $BaTiO_3$ on Ru(0001), as reported in this issue by Zollner et al.[31] This indicates the broader concept of OQC and approximants in the field of perovskites on metal substrates.

The large unit cell approximant shown in Figure 11c has been discovered in the $SrTiO_3$/Pt(111) system.[7] Its unit cell includes all motifs that are essential for the description of the OQC tiling. In addition to the three basic building blocks, even the characteristic dodecagon is part of the unit cell. In total it contains 36 tiles and 24 Ti atoms. Anticipating the similar stoichiometry as reported for the σ-phase approximant of $Ba:Ti:O = 1:1:2.5$, the large unit cell approximant contains 108 atoms in the unit cell.[28,29] Similar to the σ-phase approximant, this large unit cell approximant is in registry with the substrate. It forms a

$$\begin{pmatrix} 9 & 0 \\ 9 & 16 \end{pmatrix}$$

superstructure with respect to Pt(111). Due to the symmetry mismatch, six domains of the approximant contribute to the LEED pattern, which is shown in **Figure 12**. At the position corresponding to the second-order diffraction of the OQC, which is marked by the red circle in Figure 12, the approximant and the OQC pattern are identical. However, a clear sixfold symmetry is seen at the positions of the third- and fourth-order OQC diffraction spots marked by the blue circles. The different domains contribute to common spots every 60° along these circles, whereas their diffraction spots are located at slightly different positions with 30° rotations in between. As a consequence, the diffraction intensities are smeared out in the reciprocal space. An additional difference to the diffraction pattern of the OQC is the much higher number of intense diffraction spots. This could be related to the substrate registry that slightly distorts the unit cell.[7] As a consequence, small deviations in lengths and angles of the tiling elements occur that might lift the prerequisites for destructive interference, which increases the number of observed spots.

Within the tiling of the $BaTiO_3$-derived OQC on Pt(111), a small number of repeating units of the large unit cell
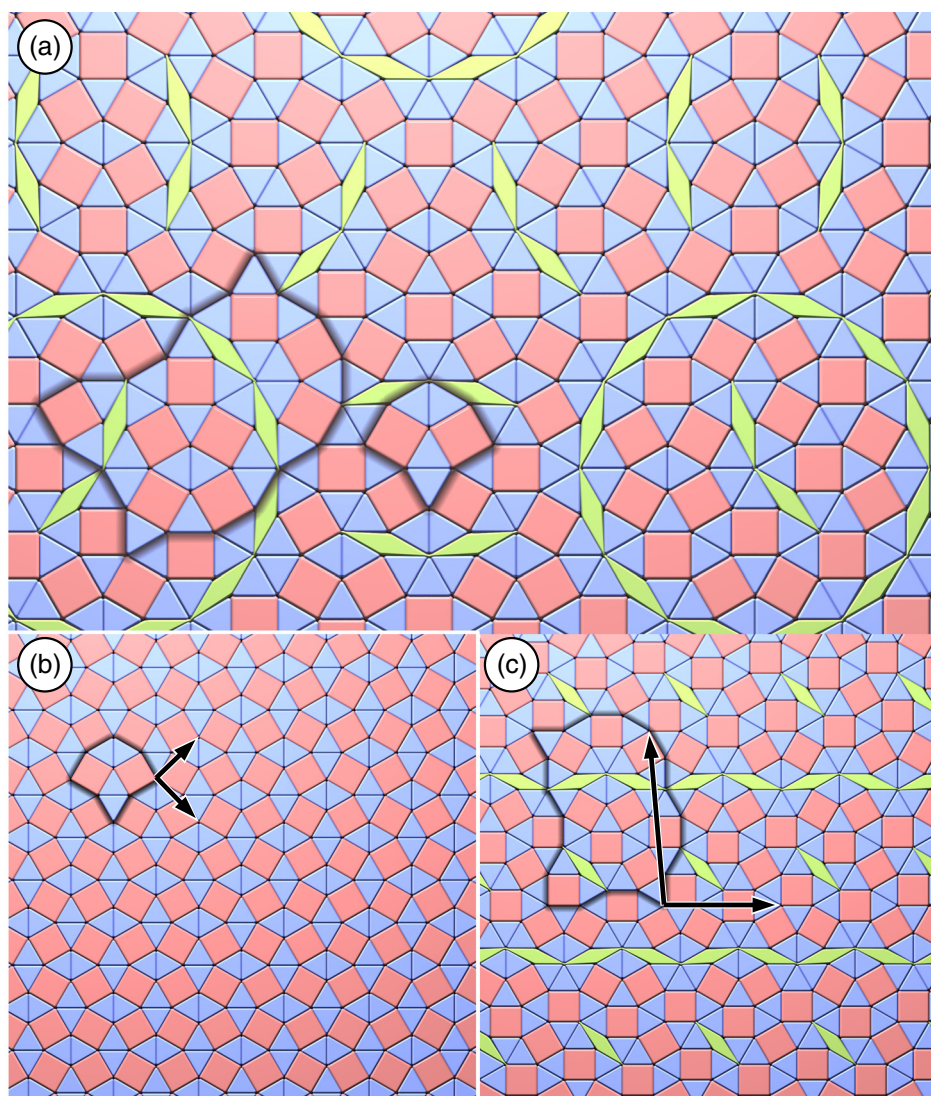
Figure 11. Illustration of the concept of the relationship of quasicrystals and their approximants. The building blocks of the OQC tiling highlighted in (a) are forming periodic structures of different unit cell dimensions (b, c). The unit vectors of the periodic structures are indicated by arrows.

approximant are locally present in multiple orientations.[21] At the current level of understanding, these units help to stabilize the epitaxial alignment of the OQC on the Pt(111) substrate.

In adddition to the two examples of approximants discussed earlier in detail, a variety of additional approximant structures is known to exist in the various combinations of ternary oxide monolayers on metal surfaces.[26,31] These experimental findings stimulated calculations that try to find a unique decoration scheme for the tiling elements to explain all observed structures.[27] Whereas this model gives interesting insights into formation of possible dodecagonal oxide structures, it fails to predict the experimentally determined 1:1 stoichiometry for Ba and Ti in the OQC and the σ-phase approximant.[28] Nevertheless, the approach to explain all observed structures by one unique decoration seems to be the key to reach a

complete understanding of the binding concept for 2D ternary oxide monolayers.

7. Conclusion and Outlook

As we discuss in this review, the field of aperiodic oxide monolayers that are formed from ternary perovskites has developed into a broad research area. All aspects and peculiarities of quasicrystals can be studied here in a textbook-like fashion for a 2D system. Especially, the combination of different diffraction techniques with real-space imaging by STM allows new insights as all atomic coordinates within a real quasicrystalline tiling are accessible and deliver via Fourier transform (FT) a microscopic picture of diffraction.
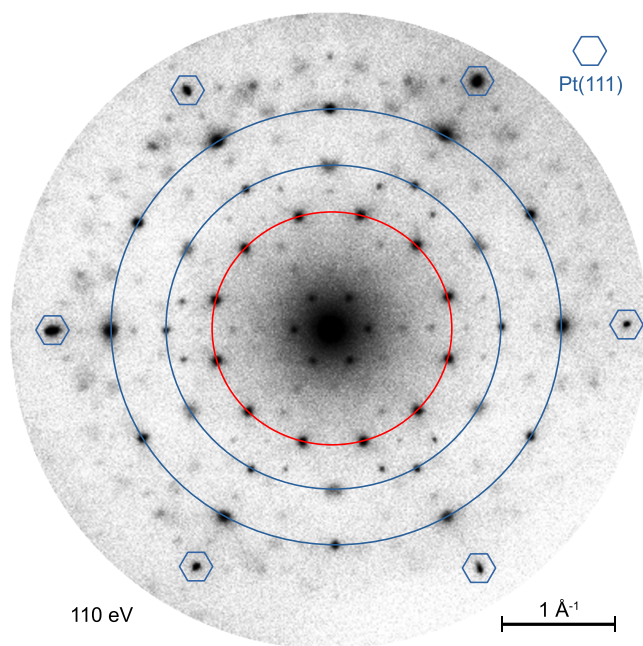
Figure 12. Diffraction pattern of the large unit cell approximant derived from $SrTiO_3$ on Pt(111).[7] The approximant forms a commensurate superstructure on the sixfold substrate. The position of the second- to fourth-order diffraction spots of the OQC is indicated by red and blue circles. Along the blue circles the sixfold symmetry induced by the superposition of six approximant domains is clearly seen.

The presence of well-defined quasicrystalline structures adds another degree of freedom to perovskite oxide interfaces beyond the formation of 2D electron gases, new forms of topology, and new ferroic coupling mechanisms.

Supporting Information

Supporting Information is available from the Wiley Online Library or from the author.

Conflict of Interest

The authors declare no conflict of interest.

[1] F. Zavaliche, T. Zhao, H. Zheng, F. Straub, M. P. Cruz, P.-L. Yang, D. Ha, R. Ramesh, *Nano Lett.* **2005**, *5*, 1793.
[2] R. Ramesh, N. A. Spaldin, *Nat. Mat.* **2007**, *6*, 21.
[3] V. Garcia, M. Bibes, L. Bocher, S. Valencia, F. Kronast, A. Crassous, X. Moya, S. Enouz-Vedrenne, A. Gloter, D. Imhoff, C. Deranlot, N. D. Mathur, S. Fusil, K. Bouzehouane, A. Barthélémy, *Science* **2010**, *327*, 1106.
[4] A. Ohtomo, H. Y. Hwang, *Nature* **2004**, *427*, 423.
[5] R. Pentcheva, W. Pickett, *Phys. Rev. B* **2006**, *74*, 035112.
[6] S. Förster, K. Meinel, R. Hammer, M. Trautmann, W. Widdra, *Nature* **2013**, *502*, 215.
[7] S. Schenk, S. Förster, K. Meinel, R. Hammer, B. Leibundgut, M. Paleschke, J. Pantzer, C. Dresler, F. O. Schumann, W. Widdra, *J. Phys. Condens. Matter.* **2017**, *29*, 134002.
[8] D. Shechtman, I. Blech, D. Gratias, J. W. Cahn, *Phys. Rev. Lett.* **1984**, *53*, 1951.
[9] L. Bendersky, *Phys. Rev. Lett.* **1985**, *55*, 1461.
[10] T. Ishimasa, H.-U. Nissen, Y. Fukano, *Phys. Rev. Lett.* **1985**, *55*, 511.
[11] N. Wang, H. Chen, K. Kuo, *Phys. Rev. Lett.* **1987**, *59*, 1010.
[12] S. Förster, J. I. Flege, E. M. Zollner, F. O. Schumann, R. Hammer, A. Bayat, K.-M. Schindler, J. Falta, W. Widdra, *Ann. Phys.* **2017**, *529*, 1600250.
[13] S. J. Tauster, S. C. Fung, R. L. Garten, *J. Am. Chem. Soc.* **1978**, *100*, 170.
[14] C. S. Ko, R. J. Gorte, *Surf. Sci.* **1985**, *161*, 597.
[15] S. J. Tauster, S. C. Fung, R. T. K. Baker, J. A. Horsley, *Science* **1981**, *211*, 1121.
[16] Z. Hu, K. Kunimori, H. Asano, T. Uchijima, *J. Catal.* **1988**, *112*, 478.
[17] Y. N. Sun, Z. H. Qin, M. Lewandowski, E. Carrasco, M. Sterrer, S. Shaikhutdinov, H.-J. Freund, *J. Catal.* **2009**, *266*, 359.
[18] O. Dulub, W. Hebenstreit, U. Diebold, *Phys. Rev. Lett.* **2000**, *84*, 3646.
[19] N. Niizeki, H. Mitani, *J. Phys. A Math. Gen.* **1987**, *20*, L405.
[20] F. Gähler, in *Proceedings of the ILL/CODEST Workshop*, World Scientific, Singapore **1988**, p. 13.
[21] S. Schenk, E. M. Zollner, O. Krahn, B. Schreck, R. Hammer, S. Förster, W. Widdra, *Acta Cryst.* **2019**, *A75*, 307.
[22] L.-G. Liao, W.-B. Zhang, T.-X. Yu, Z.-X. Cao, *Chin. Phys. Lett.* **2013**, *30*, 026102.
[23] C.-T. Chiang, M. Ellguth, F. O. Schumann, C. Tusche, R. Kraska, S. Förster, W. Widdra, *Phys. Rev. B* **2019**, *100*, 125149.
[24] E. M. Zollner, S. Schenk, M. Setvin, S. Förster, *Phys. Stat. Sol. B* **2019**, https://doi.org/10.1002/pssb.201900620.
[25] E. M. Zollner, S. Schenk, S. Förster, W. Widdra, *Phys. Rev. B* **2019**, *100*, 205414.
[26] S. Förster, K. Meinel, K.-M. Schindler, W. Widdra, *Surf. Interface Anal.* **2012**, *44*, 628.
[27] E. Cockayne, M. Mihalković, C. L. Henley, *Phys. Rev. B* **2016**, *93*, 020101(R).
[28] S. Förster, M. Trautmann, S. Roy, W. A. Adeagbo, E. M. Zollner, R. Hammer, F. O. Schumann, K. Meinel, S. K. Nayak, K. Mohseni, W. Hergert, H. L. Meyerheim, W. Widdra, *Phys. Rev. Lett.* **2016**, *117*, 095501.

ADVANCED
SCIENCE NEWS

www.advancedsciencenews.com

physica
pss status solidi **b**

www.pss-b.com

[29] K. Mohseni Roy, S. Förster, M. Trautmann, F. Schumann, E. Zollner, H. Meyerheim, W. Widdra, *Z. Kristallogr.* **2016**, *231*, 749.

[30] K. Mohseni, H. L. Meyerheim, *Phys. Stat. Sol. B* **2019**, https://doi.org/10.1002/pssb.201900605.

[31] E. M. Zollner, F. Schuster, K. Meinel, P. Krause, S. Schenk, B. Allner, S. Förster, W. Widdra, *Phys. Stat. Sol. B* **2019**, Unpublished.

[32] S. Förster, W. Widdra, *Surf. Sci.* **2010**, *604*, 2163.

[33] S. Förster, W. Widdra, in *Oxide Materials at the Two-Dimensional Limit*, (Eds: F. P. Netzer, A. Fortunelli), Springer, Cham, Switzerland **2016**, Ch. 13.

[34] F. Schumann, K. Mohseni, S. Förster, E. M. Zollner, R. Felici, W. A. Adeagbo, W. Hergert, H. L. Meyerheim, W. Widdra, Unpublished.

[35] H. T. Evans Jr., R. D. Burbank, *J. Chem. Phys.* **1948**, *16*, 634.

[36] M. Muntwiler, J. Zhang, R. Stania, F. Matsui, P. Oberta, U. Flechsig, L. Patthey, C. Quitmann, T. Glatzel, R. Widmer, E. Meyer, T. A. Jung, P. Aebi, R. Fasel, T. Greber, *J. Synchrotron. Radiat.* **2017**, *24*, 354.

[37] L. T. Hudson, R. L. Kurtz, S. W. Robey, D. Temple, R. L. Stockbauer, *Phys. Rev. B* **1993**, *47*, 1174.

[38] W. Göpel, J. A. Anderson, D. Frankel, M. Jaehnig, K. Phillips, J. A. Schäfer, G. Rocker, *Surf. Sci.* **1984**, *139*, 333.

[39] J. T. Mayer, U. Diebold, T. E. Madey, E. Garfunkel, *J. Electron Spectrosc. Relat. Phenom.* **1995**, *73*, 1.

[40] F. Sedona, G. A. Rizzi, S. Agnoli, F. X. Llabrés i Xamena, A. Papageorgiou, D. Ostermann, M. Sambi, P. Finetti, K. Schierbauk, G. Granozzi, *J. Phys. Chem. B* **2005**, *109*, 24411.

[41] G. Barcaro, S. Agnoli, F. Sedona, G. A. Rizzi, A. Fortunelli, G. Granozzi, *J. Phys. Chem. C* **2009**, *113*, 5721.

[42] D. Ragazzon, A. Schaefer, M. H. Farstad, L. E. Walle, P. Palmgren, A. Borg, P. Uvdal, A. Sandell, *Surf. Sci.* **2013**, *617*, 211.

[43] M. H. Farstad, D. Ragazzon, H. Grönbeck, M. D. Strømsheim, C. Stavrakas, J. Gustafson, A. Sandell, A. Borg, *Surf. Sci.* **2016**, *649*, 80.

[44] S. Doniach, M. Sunjic, *J. Phys. C Solid State Phys.* **1970**, *3*, 285.

[45] P. Lutz, S. Moser, V. Jovic, Y. J. Chang, R. J. Koch, S. Ulstrup, J. S. Oh, L. Moreschini, S. Fatale, M. Grioni, C. Jozwiak, A. Bostwick, E. Rotenberg, H. Bentmann, F. Reinert, *Phys. Rev. Mater.* **2018**, *2*, 094411.

[46] N. G. de Bruijn, *Indagationes Math.* **1981**, *43*, 38.

[47] P. Kramer, R. Neri, *Acta Cryst. A* **1984**, *40*, 580.

[48] T. Janssen, *Phys. Rep.* **1988**, *168*, 55.

[49] P. Bak, *Phys. Rev. Lett.* **1985**, *54*, 1517.

[50] J. E. S. Socolar, T. C. Lubensky, P. J. Steinhardt, *Phys. Rev. B* **1986**, *34*, 3345.

[51] M. Widom, *Phil. Mag.* **2008**, *88*, 2339.

[52] A. Yamamoto, *Acta Cryst.* **1996**, *A52*, 509.

[53] B. Grünbaum, G. C. Shepard, *Math. Magazine* **1977**, *50*, 227.

[54] J. Kepler, *Harmonices Mundi*, Linz, **1619**.

1900624 (11 of 11)